Evidence of phytoplankton light acclimation to periodic turbulent mixing along a tidally dominated tropical coastline.

M.J. McLaughlin[1,2]*, J. Greenwood[1], P. Branson[1,2], M.J. Lourey[3], C.E. Hanson[4]

[1]CSIRO Oceans and Atmosphere, Indian Ocean Marine Research Centre, M097, 64 Fairway, Crawley, Western Australia 6009

[2]University of Western Australia, Oceans Institute, Indian Ocean Marine Research Centre, M470 35 Stirling Highway, Crawley, Western Australia, 6009.

[3]BMT Global, 4/20 Parkland Rd, Osborne Park, Western Australia 6017, Australia

[4]Department of Education WA, 151 Royal Street, East Perth, Western Australia, 6004

* Corresponding author: Tel.: +61-8-9333-6523. E-mail address: james.mclaughlin@csiro.au

* ORCHID ID - 0000-0002-9936-1919

Key Points

- Variations to vertical mixing & light attenuation drives partitioning of phytoplankton taxa through differing photo-acclimation strategies.
- Offshore phytoplankton acclimated to dark conditions with strong photo-inhibition at a deep chlorophyll maximum.
- Nearshore/estuarine phytoplankton photo-acclimated to high light with elevated photosynthetic rates and no observed photo-inhibition.

Abstract

One of the largest tropical tidal ranges in the world occurs in King Sound, a semi-enclosed embayment in the tropical Kimberley region of Western Australia. Incubations of phytoplankton within King Sound displayed reduced photosynthetic efficiency, elevated maximum photosynthetic rates, and no measurable photo-inhibition. A response typical of high light adapted phytoplankton despite decreased water clarity and low ambient nutrient concentrations in the estuary. This is in contrast with the adjacent shelf where phytoplankton, associated with a deep chlorophyll maximum, display high photosynthetic efficiency, and strong light inhibition typical of low light adaptation. Remote sensing and numerical modelling suggest that spatial and temporal variations in tidal mixing drive changes in light variability and in photo-acclimation. In King Sound phytoplankton experience the largest variations in light over short timescales where diatoms dominate since they can rapidly acclimate to water column light conditions by adjusting pigment within the cell. The photo-physiological response of the phytoplankton in the Sound, suggests that acclimation to alternate weak and strong mixing exposes them to cyclical changes in light intensity delaying the onset of photo-inhibition, allowing higher maximum photosynthetic rates to be attained. These findings highlight the importance of a multifaceted approach to understanding the links between physics and photo-acclimation strategies employed by phytoplankton to more accurately determine rates of depth-integrated productivity in complex coastal areas.

Plain Language Summary

The Southern Kimberley Coast in Australia's Northwest is dominated by the largest tides in the world's tropical regions, and second only to the Bay of Fundy in Canada. King Sound the main feature of this region, is a 100-km-long, semi-enclosed embayment opening to the Indian Ocean. Tidal mixing is an important control on phytoplankton distribution in shallow coastal macrotidal regions like this. Despite low ambient nutrients and decreased water clarity in King Sound, phytoplankton showed a photo-acclimation strategy suited to high light exposure. This is in contrast with the adjacent shelf where phytoplankton, associated with a deep chlorophyll maximum, displayed a photo-acclimation strategy more suited to low light. King Sound experiences the largest variations in light over short timescales and we found the phytoplankton were dominated by diatoms since they can rapidly adjust pigment within the cell to acclimate to water column light conditions. Observations from remote sensing and numerical modelling suggest that spatial and temporal variations in tidal mixing drive changes in light variability and in photo-acclimation. The acclimation by phytoplankton to alternate weak and strong mixing exposes them to cyclical changes in light intensity delaying the onset of photo-inhibition, allowing higher maximum photosynthetic rates to be attained.

1 Introduction

Tidal mixing is an important control on phytoplankton distribution in estuaries (Cloern, 1991; Lucas *et al.*, 1999; Trigueros & Orive, 2000) and in shallow coastal macrotidal regions of the coastal sea (Blauw *et al.*, 2012, Houliez *et al.*, 2013). Tides induce horizontal and vertical mixing, which redistributes phytoplankton and nutrients, influencing community structure and phytoplankton population dynamics (Lewitus *et al.*, 1998; Domingues *et al.*, 2010). Despite several observations of tidally driven variability in estuarine phytoplankton biomass and taxonomic composition (Jouenne *et al.*, 2005; Wetz *et al.*, 2006; Domingues *et al.*, 2010; Blauw *et al.*, 2012), the impact of tides on phytoplankton productivity has not been well investigated. Measurements of phytoplankton photosynthetic rates are critical to provide accurate predictions of primary production and biogeochemical processes, important components of carbon cycling, under the variable conditions that commonly define estuarine and coastal marine environments. Here, we are primarily concerned with the effect that vertical tidal mixing has on phytoplankton photo-physiology, and its implicit effect on the overall rate of carbon fixation.

The importance of photo-acclimation in aquatic phototrophs stems from the extreme spatial and temporal variability of the underwater light field (Dubinsky & Stambler, 2009). Photo-acclimation in a phytoplankton cell is characterized by changes in the amount and ratios of light harvesting and photoprotective pigments, in photosynthetic parameters, photosynthetic and respiratory enzymatic activities, chemical composition and cell volume (Falkowski & LaRoche, 1991). Chloroplast size and morphology (shape and structure), numbers, and distribution within the cell, can be hugely different in the various phytoplankton classes and pigment-groups (Kirk & Tilney-Bassett, 1978; Larkum & Vesk, 2003). The species-specific differences in chloroplast size and morphology in a given species is also affected by light climate (irradiance, the spectral composition of irradiance and day length). In the aquatic environment these are amplified by the superimposed steep attenuation of light by water and the substances and particles dissolved and suspended in it (Smith & Mobley, 2008). Vertical turbulent mixing of the water column can modify this situation by redistributing particles, such as phytoplankton cells or suspended sediment, and altering the upward flux of nutrients relative to the vertical light gradient. This enables cells to either escape prolonged periods near the surface where photo-inhibition can occur or prevent them from sinking below the photic

zone (Demers *et al.*, 1986). Finely coordinated mechanisms of photo-acclimation allow aquatic phytoplankters to survive over a 2 order of magnitude range of ambient irradiance. Photo-acclimation to low light requires adequate nutrient supply (Herzig & Falkowski, 1989, Berges *et al.*, 1996, Cardol *et al.*, 2008) whereas cells that successfully acclimate to high light have difficulties in maintaining Redfield ratios through sufficient nutrient uptake to keep up with the fast influx of carbon (Berman-Frank & Dubinsky, 1999). Therefore, the optimal depth for phytoplankton growth is generally determined by the interrelationship between opposing vertical gradients in light intensity and nutrient concentration.

The intensity and timing of tidally induced vertical mixing can influence phytoplankton photo-physiology and overall productivity, as a result of changes in cell light history (Falkowski, 1980), and nutrient availability. Phytoplankton, in particular diatoms, can compensate for lower light conditions by rapidly synthesising more chlorophyll-*a* (chl-*a*) pigment within the cell (Sathyendranath *et al.*, 2004). When vertical mixing is moderate, the environmental conditions change at a rate slower than the physiological adaptation time of the phytoplankton, and the cells can continuously adapt their metabolism to these new conditions (Vincent, 1980). This can, for example, lead to vertical structure in phytoplankton within otherwise density uniform ocean layers (Calbet *et al.*, 2015). However, when vertical mixing is persistent and sufficiently intense, and environmental conditions change faster than the physiological adjustment time of phytoplankton, the cells tend to adjust toward average environmental conditions (Savidge, 1979; Falkowski, 1980). The physiological strategies that phytoplankton adopt in different mixing scenarios are important for maximizing the efficiency of utilization of available light and photosynthetic activity (Auclair *et al.*, 1982).

The Kimberley region in the tropical North-west of Australia is a remote and biologically diverse oceanic habitat. Semidiurnal, barotropic tides (Holloway *et al.*, 2001) interact with the wide (~300 km) shelf to produce the second largest tidal range (up to 11 m) in the world (after Canada's Bay of Fundy; Wolanski & Spagnol, 2003). The large tidal range generates strong currents (0.5 - 2 m s^{-1}; Anon, 1972). One of the largest topographical features of the southern Kimberley coast is King Sound (Fig. 1), a 100-km-long, semi-enclosed embayment. The Sound is characterised by extensive areas of shallow water with a mean depth of 18 m, but near the mouth there is a 50 m-deep 20-km-wide channel.

McLaughlin *et al.* (2019) found in April/May 2010, that the waters near the mouth of King Sound, were a phytoplankton productivity “hot-spot” despite low ambient nutrient concentration and reduced water clarity compared with the adjacent shelf. Here, we investigate the reason for the enhanced phytoplankton productivity within King Sound by comparing the photo-physiology of phytoplankton cells collected in the Sound, with those collected in shelf waters. We present photo-physiological data collected at different phases of the spring-neap (MSf) tidal cycle, and at different vertical water-column positions, across the continental shelf including locations within King Sound. We also use satellite data and results from a numerical model to help characterise the tidal mixing conditions in the region, and phytoplankton pigment data to identify the dominant phytoplankton species.

2 Materials and Methods

2.1 Oceanographic sampling

Three cross-shelf transects were occupied during an oceanographic cruise (subsequently referred to as SS2010) off the south-eastern section of the Kimberley coast in proximity to King Sound (KS) (13.5 - 17°S, 120 - 124°E; Fig. 1) in austral autumn (14 April - 5 May 2010). A central transect that extended into KS was sampled twice; once on the rising spring tide, and again on the falling neap tide approximately two weeks later. A northern and a southern transect provided greater spatial coverage of the shelf, with the northern transect (Fig. 1; stations 27, 45 and 46) sampled 1.5 days following the spring-tide maximum, and the southern transect (Fig. 1; stations 121, 109 and 101) sampled between 3 and 5 days following the neap tide.

To evaluate cross-shelf differences in phytoplankton photo-physiology, locations near the 50 m (inner shelf), 200 m (mid-shelf), and 1000 m (outer-shelf) isobaths were sampled on each transect. On the central transect excursions into KS were made where a further two stations were sampled on the spring tide (Fig 1. stations 24 and 25) and two stations during the neap (Fig 1. stations 84 and 85). Water samples were collected using a 24 x 10 L Niskin bottle rosette with profiles of conductivity and temperature (Seabird SBE

9/11 dual-sensor unit), photosynthetically active radiation (PAR 400–700 nm; Biospherical Instruments QCP-2300), and fluorescence (Chelsea Instruments Aquatracka™ fluorometer) calibrated with extracted chlorophyll samples collected from the water column. Water samples from the production cast at each station were collected from between 3 and 5 nominal depths (surface [~ 2 m], 10 m, 25 m, 50 m, 75 m) dependent upon the bottom depth, and analysed for primary production (PP) in addition to chl-*a* and phytoplankton community structure via high performance liquid chromatography (HPLC).

Vertical PAR profiles for each production cast were obtained from the on-site CTD cast closest to the sun's zenith. Light profiles collected at some other nearby shelf locations occupied during the same cruise (Cherukuru *et al.*, 2019) were added to provide additional information about the underwater light climate on the continental shelf. Linear regression of the natural logarithm of PAR versus water-depth confirmed exponential light decay in most cases providing a value of the attenuation rate k_d. For the PAR profiles collected in King Sound the surface irradiance measured on the deck of the ship was used to provide an additional in-water value at a nominal depth of 1 m after adjusting for sun angle and 7.6% rapid attenuation following the approach of Morel (1991). Euphotic depth (z_{eu}) was calculated as the water depth where irradiance is reduced to 1% of the surface value as $z_{eu} = \ln(0.01) / k_d$. We note that this is a somewhat conservative estimate of the ocean's true euphotic zone (Marra et al. 2014), but it nevertheless provides a useful reference for this study. For stations 24, 25, 84 and 85 occupied within King Sound the median and mean PAR were also calculated according to the formulations given by Berenhfeld (2015) (median) and Blain *et al.* (2013) (mean) and using a daily mean near-surface irradiance of 500 µE m^{-2} s^{-1} based on mean daily records of incident PAR collected during the cruise and adjusted for sun angle and 7.6% rapid attenuation at the water surface. Mixed-layer depth (l) was calculated as the depth where the value of the potential density unit (σ_θ), is offset by + 0.03 kg m^{-3} compared with the value at 10 m (de Boyer-Montegut *et al.*, 2004). For locations within King Sound where σ_θ remained above this threshold throughout the water-column, the mixed-layer was assumed to extend to the seabed. The implied lack of any vertical density stratification in these cases was confirmed by visual examination of the vertical profile of σ_θ.

2.2 Satellite remote sensing and hydrodynamic model analysis

Satellite remote sensing data were obtained from the Integrated Marine Observing System (IMOS) and analysed in conjunction with output from a three-dimensional numerical hydrodynamic model developed for the Western Australian Marine Science Institute (WAMSI). To identify the extent of persistent vertical tidal mixing on the continental shelf, the spatial gradient in night-time climatological Sea Surface Temperature (SST) was also calculated from the Sea Surface Temperature Atlas of the Australian Regional Seas (SSTAARS) published in Wijffels *et al.* (2018).

In northern Australia, vertical mixing by the strong tidal currents act as a sink for heat and freshwater input at the ocean surface. Assuming that in a given region the mixing efficiency and bed friction coefficients are constant the location of the front should be defined by a critical value of h/u^3, where h is the water depth and u is the surface tidal velocity amplitude (Simpson & Hunter, 1974). We utilized the results from a three-month simulation with the Regional Ocean Modelling System (ROMS) to calculate the surface tidal velocity amplitude as $u = u_{M2} + u_{S2}$ where u_{M2} and u_{S2} are the amplitude of the semi-major tidal ellipses for the M_2 and S_2 tidal constituents from a harmonic fit of the modelled surface current. The ROMS model utilized 30 uniformly spaced vertical sigma layers and included forcing from surface heat fluxes, freshwater input from coastal catchments and applied the k-ϵ turbulence closure scheme with a quadratic bed friction coefficient of 3×10^{-3}. For further details of the model configuration and validation see Feng *et al.* (2017).

Lewis *et al.* (1984) present a simple model that compares the relative magnitudes of the timescales of photoadaptation to the timescales of irradiance fluctuations due to vertical mixing. To assess the influence of vertical tidal mixing on the observations of plankton photo-physiology we estimated a mixing timescale from the ROMS simulation as $T_M = l^2/K_z$ where K_z is the modelled vertical turbulent diffusivity (with units m^2/s) and l is the thickness of the mixed layer. On continental shelves with large tides, increases in vertical mixing during the spring tide are accompanied by increases in suspended sediment due to the increased bed shear stress. At in-situ sample locations estimates of the light attenuation coefficient (k_d at 490 nm) were obtained from the MODIS ocean colour satellite record from 2002 – 2020 available from IMOS (2020). At each station a harmonic fit of the water surface elevation from the ROMS model was calculated to provide a 20-year timeseries of predicted tide for each station. Observations of cloud-free pixels within 2 km

of each station were classified according to the tidal phase of the semi-diurnal (high water, ebb tide, low water and flood tide) and spring-neap (spring, falling, neap and rising) cycles at the time of pixel acquisition (see Fig. S1). Within each tide phase class, the mean and standard deviation of k_d was calculated to provide an estimate of changes in irradiance length scale ($k_d{}^{-1}$) compared to the mixing length scale (l).

2.3 Phytoplankton pigment analyses

One litre of seawater from each depth was vacuum-filtered onto a Whatman 25 mm diameter glass fibre filter (GF/F) (nominal pore size of 0.7 µm) and analysed for chl-*a* and phaeopigment (represents the total chl-*a* fraction). The filters were stored at -20°C until analysis (24 - 48 hours post-collection), when pigments were extracted in 90% acetone overnight and analysed using a calibrated Turner Designs model 10AU fluorometer and the acidification technique of Parsons *et al.* (1989).

Between 1-5 L of the surface water sample were filtered onto a 25 mm, 0.7 µm, Whatman GF/F and stored in liquid nitrogen until analysis. Phytoplankton pigments were extracted and analysed by High Performance Liquid Chromatography (HPLC) with a Waters-Alliance system following the CSIRO protocol detailed in Hooker *et al.*, (2009). In this study (as per Clementson *et al.*, 2004) pigments that relate specifically to an algal class are termed marker or diagnostic pigments (Jeffrey & Vesk, 1997). Some of these diagnostic pigments are found exclusively in one algal class (e.g. alloxanthin which is only found in cryptophytes) while others are the principal pigments of one class but are also found in other classes (e.g. fucoxanthin in diatoms and some haptophytes). The presence or absence of these diagnostic pigments can provide a simple guide to the composition of a phytoplankton community including identifying classes of small flagellates that cannot be determined by light microscopy techniques. In this study the presence of fucoxanthin has been used to indicate diatoms; peridinin - dinoflagellates; 19’ - hexanoyloxyfucoxanthin (19HF) haptophytes; alloxanthin - cryptophytes; prasinoxanthin - prasinophytes; lutein - chlorophytes; zeaxanthin - cyanobacteria and 19’-butanoyloxyfucoxanthin – pelagophytes (Vidussi *et al.*, 2001).

2.4 Laboratory incubations

During the voyage, a total of 58 phytoplankton primary production versus irradiance experiments were conducted at discreet water depths for 15 locations across the continental shelf including King Sound (Fig. 1). The results from these experiments were used to characterise changes in phytoplankton photo-physiology reported here and calculate depth-integrated primary production rates reported by McLaughlin *et al.* (2019).

A small volume (7 mL) ^{14}Carbon (^{14}C) uptake method was used with a photosynthetron incubator (Lewis & Smith 1983; Mackey *et al.*, 1995, 1997). Water samples collected during night-time casts were stored at cool temperature in the dark until processing and incubation on the following day. A working solution for each depth was created by inoculating sample water with ^{14}C (as $NaH^{14}CO_3$) to a final concentration of 1.0 µCi per 1.0mL seawater. Duplicate aliquots from each sampling depth were incubated for approximately 1 h at seven main light levels, ranging from 0 to 750 $\mu Em^{-2}\ s^{-1}$, by using combinations of spectrally resolving blue filters (LEE Filters # 119, 201, 202, and 203; for detailed wavelength specifications see http://www.leefilters.com/lighting/colour-list.html). Duplicates were exposed to slightly different irradiance levels by variability in the light output through distance between the light tubes with actual irradiance levels (measured using a Biospherical Instruments Inc. 2100 PAR logger) used in the analyses to account for inherent variability in the light output between the light tubes. Two 100 µL aliquots from each depth were analysed to determine the total initial activity, as were duplicate 7mL time zeros (Mackey *et al.*, 1995). Continuous surface seawater flow through the photosynthetron was used to regulate the temperature for all incubations. Experiments were terminated through the addition of 0.25mL of 6M HCl and placing the samples in an orbital shaker at ~180 revs min^{-1} for ca. 24 h to drive off any excess ^{14}C as CO_2 (Mackey *et al.*, 1995). All samples were counted on-board the ship using an LKB Rackbeta liquid scintillation counter the following day.

The model of Platt *et al.* (1980) was successfully fit to the majority of the photosynthesis-irradiance data using the Matlab © function *nlinfit* according to

$$P = P_s\left(1 - e^{-\alpha I / P_s}\right)e^{-\beta I / P_s} \quad (1)$$

Where P is chlorophyll *a* specific photosynthesis in units of mg C mg Chl-*a*$^{-1}$ hr^{-1}, P_S is the light saturated photosynthetic rate in the absence of photo inhibition in units of hr^{-1}, α (photosynthetic efficiency) is the initial slope of the productivity irradiance response in units of [mg C mg Chl-*a*$^{-1}$ h^{-1} µEm^2 s], β is an index of photo inhibition (same units as α), and I is irradiance in µEm^{-2} s^{-1}. The maximum photosynthetic rate, $P_{\max}$ is calculated as

$$P_{\max} = P_s\left[\alpha/(\alpha+\beta)\right]\left[\beta/(\alpha+\beta)\right]^{\beta/\alpha} \quad (2)$$

For the data collected within King Sound, the fitting of equation 1 failed due to scatter in the rate data collected at high light intensities, and lack of any clear evidence of light inhibition, making estimation of the model parameters uncertain. In these cases, a simplified model was easily fitted to the data by assuming β equal to zero

$$P = P_s\left(1 - e^{-\alpha I/P_s}\right) \quad (3)$$

Where P_S is numerically equal to $P_{\max}$, and α retains its earlier meaning. Successful fitting of equation 3, in cases where equation 1 had previously failed, reflected a general absence of any noticeable photo-inhibition in the data.

3. Results

3.1 Euphotic and mixed-layer depths

Vertical profiles of σ_θ, and PAR show that, except at some of the KS and 50 m stations, the euphotic depth is greater than the mixed-layer depth, and generally increases with distance offshore (Fig. 2). The lack of any significant vertical gradient in water density or chl-*a* concentration suggests that all KS stations were vertically well-mixed at the time of sampling (Fig. 3). This finding is consistent with the mixed-layer extending to the seabed at all KS stations. The gradient of the natural logarithm of PAR versus depth suggested differences in water clarity on different phases of the MS_f tidal cycle, with steeper slopes on the spring tide indicating light attenuation was higher (Fig. 3). *In-situ* light attenuation also tended to be stronger at the deeper KS stations 24 and 84 than the shallower stations 25 and 85 located further upstream. The

combination of deeper water and stronger light attenuation resulted in the euphotic depth at the deeper KS stations 24 and 84 being 18 and 14 m shallower than the seabed respectively, while the shallower KS stations 25 and 85 further upstream had euphotic layers that extended over most of the water-column. Calculations of mean and median PAR at the KS stations emphasize these differences with the mean water-column PAR intensity approximately 1.5 times greater, and the median PAR intensity 4 or 5 times greater at the shallower upstream sites (Table 1).

3.2 Tidal mixing on the continental shelf

On the continental shelf in the Kimberley Region tidal mixing plays a significant role in breaking down stratification for depths shallower than 50 m. In Northern Australia, persistent cold patches have been found to coincide with regions with significant variability in SST over the spring/neap cycle and coincide with regions that have suppressed both seasonal and non-seasonal variance in SST (Wijffles *et al.*, 2018). Studies of SST fronts in regions where tidal mixing is significant suggest that tidal mixing dominates for $h/u^3 < 50$ with SST fronts observed for $65 < h/u^3 < 100$. On the Kimberley shelf region gradients in SST climatology larger than 1^o C per degree of latitude occur along the 50 m contour and correspond with the region $65 < h/u^3 < 100$ calculated from the ROMS numerical model (Fig. 4). During spring tides, the temperature front in the proximity of the 50 m contour corresponds to a numerically modelled mixing timescale (T_M) of 24 hours (taking l as the water depth). For areas shallower than the 50 m depth, T_M < 24 hours during spring tides. For shelf regions where the depth is greater than 50 m, surface mixing (due to the wind) become the dominant process driving mixing within the euphotic zone.

3.3 Phytoplankton community composition

Within King Sound (CTD stations 24–25, 84–85), the phytoplankton community was dominated by diatoms as indicated by the relatively high concentrations of fucoxanthin (~30 to 55% of mean relative pigment contribution). On the adjacent shelf, the community was increasingly dominated by cyanobacteria and haptophytes with distance offshore, according to the relative increase in zeaxanthin and hexanoyloxyfucoxanthin concentrations compared with other pigments (Fig. 5).

297

298 *3.4 Phytoplankton light response curves*

299 The photo-physiological (PI) response on the mid- and outer-shelf (Fig. 6; Table 2), where phytoplankton
300 mainly grow in a sub-surface layer (McLaughlin *et al.*, 2019), is typical of observations made elsewhere in
301 the open-ocean where the lack of available nutrients at the surface tends to limit phytoplankton growth to
302 the base of the euphotic layer (Hanson *et al.*, 2007). Under these conditions the phytoplankton in the study
303 region displayed relatively high photosynthetic efficiency with a median value of 0.121 mg C mg chl-a^{-1} h^{-1}
304 μEm^2 s ($0.064 \leq \alpha \leq 0.239$), and relatively strong light inhibition with a median value of 0.017 mg C mg chl-
305 a^{-1} h^{-1} µE m^2 s ($0.005 \leq \beta \leq 0.047$), typical of low light adapted phytoplankton (Demers *et al.*, 1986). The PI
306 response at depths less than the estimated mixed layer tended to be similar (Table 2; Fig. 6), whereas
307 below the mixed layer vertical variation in the PI response was more noticeable with maximum
308 photosynthetic rates reducing, and the onset of photo-inhibition occurring at lower light intensities, with
309 increasing water-depth (Table 2; Fig. 6). Maximum photosynthetic rates on the mid- and outer-shelf ranged
310 from 1.410 to 9.564, with a median value of 5.177 mg C mg chl-a^{-1} h^{-1} (Table 2).

311

312 In contrast, the phytoplankton PI response in KS displayed a reduced median photosynthetic efficiency of
313 0.075 mg C mg chl-a^{-1} h^{-1} μEm^2 s ($0.056 \leq \alpha \leq 0.175$), an elevated median maximum photosynthetic rate of
314 8.889 mg C mg chl-a^{-1} h^{-1} ($4.554 \leq P_{\max} \leq 14.589$), and lack of any pronounced photo-inhibition compared
315 with the shelf, (Fig. 7; Table 2), typical of light-acclimated phytoplankton (Demers *et al.*, 1986). The highest
316 maximum photosynthetic rate was observed in KS under spring tide conditions at station 24 with values
317 ranging from 9.320 to 14.589 mg C mg chl-a^{-1} d^{-1} between the surface and 25 m water depth (Fig. 7).
318 Similar results were obtained at the equivalent location during neap tide conditions (station 84) with values
319 of P_{max} estimated to be between 9.704 and 13.689 mg C mg chl-a^{-1} d^{-1} (Fig. 7). At stations 25 and 85,
320 located in shallower water further upstream, values of $P_{\max}$ were significantly reduced with median values
321 of 7.718 ($7.341 \leq P_{\max} \leq 8.458$) and 4.762 ($4.554 \leq P_{\max} \leq 5.068$) mg C mg chl-$a^{-1}$ d^{-1} respectively, and also
322 displayed reduced vertical variability compared with stations 24 and 84 (Fig. 7; Table 2).

323

Results for the inner-shelf returned the lowest median values of both photosynthetic efficiency 0.048 (0.03 ≤ α ≤ 0.114) mg C mg chl-a^{-1} h^{-1} µEm^2 s , and maximum photosynthetic rate 3.8215 (3.021 ≤ $P_{\max}$ ≤ 10.223) mg C mg chl-a^{-1} d^{-1} with weak rates of photo-inhibition 0.004 (0.000 ≤ β ≤ 0.004) mg C mg chl-a^{-1} h^{-1} µEm^2 s compared with shelf positions further offshore and with stations inside KS (Figs. 6 & 7; Table 2). Very little vertical variation in the PI response was observed on the inner shelf at stations 17 and 121, where the mixed layer was estimated to extend to the seabed (Table 2; Fig. 6). In contrast, the relatively shallow mixed-layers of 15 m and 18 m observed at stations 27 and 87 respectively corresponds with observed vertical separation in the PI response at 0 and 10 m from the response at 25 and 50 m (Table 2; Fig. 6).

3.5 Relative importance of tidal mixing on phytoplankton photoadaptation

Lewis *et al.* (1984) proposed a simple model to compare the (order of magnitude) importance of photo-acclimation compared to vertical turbulent mixing based on a 1-D reaction-diffusion model. Assuming that vertical variations with depth of phytoplankton photo-adaptive parameters are due to acclimation to the local light climate, the dimensionless groups that control photo-acclimation are the irradiance aspect ratio $k_d l$ and the relative mixing timescale $K_z \gamma / l^2$ where γ is the acclimation timescale of the photo-adaptive parameter under consideration. The modulation of the M_2 tide across the spring neap cycle results in variations in both vertical mixing and light attenuation due to enhanced bed shear stress and resuspension of seabed sediment. Figure 8 presents the variation in photo-acclimation regime derived from MODIS estimates of $k_d = k_{490}$ (IMOS, 2020) and vertical mixing from the ROMS model. For KS stations l is taken as the local water depth and for all other stations l is taken to be nominally 40 m (Fig. 8). In KS vertical turbulent mixing is dominant for photo-acclimation timescales greater than approximately 4 hours (Fig. 8a) across the spring neap cycle. Timescales of vertical mixing in KS are consistent across the two stations (Table 1), despite their differing depth due to vertical mixing scaling with the water depth in shallow open channel flow (Fischer, 1963). However, spatial and temporal variations in light attenuation result in differing light climates with station 24/84 having greater vertical variations in light (over a mixing timescale) than station 25/85. At stations on the 50 m depth contour, photo-acclimation dominates vertical mixing for adaptation timescales shorter than approximately 24 hours across the spring neap cycle. Depending on the

location, mixing timescales can vary by an order of magnitude across the spring neap cycle, with station 121 exhibiting the largest variation across the MS_f cycle. At stations further offshore photo-acclimation dominates vertical mixing and vertical variations in photo-adaptive parameters are expected.

4. Discussion

King Sound has been identified as a pelagic productivity 'hotspot', despite reduced water clarity and low ambient nutrient concentration compared with the adjacent shelf (McLaughlin *et al.*, 2019). Closer investigation of the photo-physiological (PI) response of phytoplankton sampled in the region reported here, suggests that photo-acclimation to periodic vertical tidal mixing, is responsible for the high rates of depth-integrated productivity measured near the mouth of King Sound. Dissolved nutrient content was low and constant with depth at the time of sampling the KS stations (McLaughlin *et al.*, 2019). We suspect that this is due to the vertical tidal mixing which delivers a continuous supply of nutrients to the surface waters in King Sound where they are taken up rapidly to support the rapid fixation of carbon (Berman-Frank & Dubinsky, 1999).

Depending on topography and tidal amplitude, dissipation of semi-diurnal (M_2) tidal energy can result in either continuous intense turbulent vertical mixing, or alternating periods of weak and relatively strong mixing at M_2 frequency. Phytoplankton have developed an array of interrelated cellular mechanisms allowing them to optimize light harvesting and utilization during exposure to changes in irradiance in a temporally and spatially dynamic light field (Dubinsky & Stambler, 2009). These responses form the phenotypic process termed photo-acclimation, which includes adjustment of optical properties involved in the ‘light reactions’ of photosynthesis. The outcome of the photo-acclimation process mitigates extreme light intensity fluctuations, reducing their effect to levels allowing growth beyond simple survival (Dubinsky & Stambler, 2009). In an environment exposed to continuous intense mixing, the light conditions experienced by phytoplankton can change faster than the physiological adjustment time of the cells, so that phytoplankton can only adjust to the average light conditions (Demers & Legendre, 1982). In contrast, phytoplankton exposed to alternating periods of weak and strong vertical mixing at M_2 frequency can respond by changing their maximum photosynthetic rates (Fréchette & Legendre, 1982), depending on their relative position in the water column compared to the vertical light gradient. Enhanced photosynthetic

activity has been observed for phytoplankton exposed to cyclical changes in light intensity, likely due to reduced exposure of cells to bright light allowing high rates of photosynthesis to be maintained before photo-inhibition occurs (Demers *et al.*, 1986). The MS_f tide modulates the amplitude of the M_2 tide changing the vertical mixing conditions for phytoplankton; spring tides will favour more continuous mixing with shorter periods of stability and stronger mixing, while neap tides will offer longer periods of stability and reduced mixing rates.

The highest rates of photosynthesis were recorded for phytoplankton sampled near the mouth of KS (Fig. 1; stations 24 and 84), with little difference between spring and neap tide conditions (Fig. 7). Low photosynthetic efficiency and absence of photo-inhibition at this location is characteristic of light-adapted phytoplankton. Characteristic mixing timescales in KS were consistent across the two stations and are significantly shorter than the M2 tide, suggesting that phytoplankton at these locations are exposed to highly variable light conditions. Cyclical variations in the phytoplankton light climate at this location are exaggerated by the fact that the photic layer covers little more than half of the total water column, meaning that during a mixing cycle (where mixing extends all the way to the seabed) the phytoplankton will spend some time in the 'dark'. Further upstream in King Sound (Fig. 1; stations 25 and 85) the mixing timescales are the same, but the increased depth-averaged PAR at these locations (Table 1) as a result of the similarity between mixing and photic depths, means that the phytoplankton experience reduced vertical variations in light over a mixing timescale than they do at the deeper KS sites 24/84. This is reflected in the vertical separation of the two main KS locations when plotted on Figure 8. We suspect therefore that a more constant light climate is the main reason for the lower maximum photosynthetic rates measured at the upstream KS sites, assuming that cyclical changes in light lead to higher maximum photosynthetic rates as argued above. However, without information about nutrient uptake rates, nutrient limitation at the upstream sites cannot be eliminated as a possible cause for the reduced photosynthetic rates. We note that, sampling in KS generally took place close to high tide to aid ship navigation, and therefore may have coincided with lower tidal velocities and lower rates of vertical mixing than experienced at other times of the M_2 tidal cycle.

409 Photo-acclimation and photo-adaptation in many cases have been used as synonyms; however, more
410 recently, acclimation is reserved for phenotypic changes taking place in response to environmental cues
411 during the lifetime of the cell, while adaptation is usually used for genomic changes occurring in a
412 population on an evolutionary time scale (Dubinsky & Stambler, 2012). Blau *et al.* (2012) observed that
413 short-term fluctuations of coastal phytoplankton were dominated by periodicities of 6 hours 12 min, 12
414 hours 25 min and 24 hours. They concluded that the tidal cycle is a major determinant of phytoplankton
415 fluctuations at several different time scales. The mixing time scale calculated during the spring tide in Kind
416 Sound was ~3.5 hours, less than the 6 hour 12 min, period of the semi-diurnal tides found by Blau *et al.*
417 (2012). From diagnostic pigments, we found the phytoplankton community in King Sound was dominated
418 by diatoms (Fig. 5), which has been shown in lab culture experiments to be adaptive to their environment
419 by changing their photosynthetic potential to meet the demands of the area (Lavaud *et al.*, 2007). Diatoms
420 also generally have higher nutrient demands than other phytoplankton species (Smetacek, 1985).
421 Consequently, frequently mixed environments with variable light conditions and high nutrient fluxes are
422 often dominated by diatoms (Demers *et al.*, 1986). In contrast, the offshore phytoplankton community was
423 dominated by smaller-celled haptophytes and cyanobacteria that have less ability to cope with a fluctuating
424 light climate as in some cases they have light specific genotypes (West & Scanlan, 1999).

425

426 Hanson *et al.* (2007) showed that small differences in light attenuation and photo-inhibition can cause a
427 shift from surface-dominated to deep chlorophyll maxima (DCM) - dominated populations, and significantly
428 affect computations of primary production. In offshore waters bathymetric separation of different taxa is
429 driven by photo-acclimation. Processes of photo-acclimation push the euphotic depth deeper where
430 photosynthetic gains surpass respiratory losses more so than would be possible without photo-acclimation
431 further down the water column (Dubinsky & Stambler, 2012). A recent assessment of the physical and
432 chemical oceanography indicated more stratified conditions offshore with a pool of nutrients observed at
433 ~70 m, and phytoplankton growth restricted to a sub-surface maximum (McLaughlin *et al.*, 2019), a similar
434 trend to that found by Hanson *et al.* (2007), and Lourey *et al.* (2012) in other areas along the Western
435 Australia coast. The observed PI response on the outer shelf (Fig. 6) is consistent with observations made
436 in similar stratified ocean conditions where phytoplankton adjust their photo-physiology for the shaded
437 conditions (Falkowski, 1984) encountered at the base of the euphotic layer. This is largely confirmed by the

relative position of the outer shelf stations in Figure 8 showing where a depth-dependant photo-acclimation would be expected in water-column conditions at the offshore sites due to the reduced mixing.

Finally, it is interesting to note that maximum photosynthetic rates appear to be somewhat restricted in the vicinity of the 50 m isobath (Fig. 6). Our analysis shows that this is a region of the shelf subject to strong variations in the mixing time-scale (Fig. 8), and has confirmed earlier work (Cresswell & Badcock, 2000) that it is associated with a tidal-mixing front distinguishing offshore stratified waters from well-mixed water on the shoreward side (Fig. 4). The extent of vertical mixing in this case is related to tidal range and can be much reduced on the neap tide (Cresswell & Badcock, 2000), which may explain the increased vertical variation in PI response, compared with the spring tide (Fig. 6). Although the existence of tidal fronts is known to affect phytoplankton physiology in various ways (Demers *et al*., 1986), further investigation will be needed to understand this particular case. The phytoplankton at the 50 m stations was composed of an almost equal mix of diatoms typical of inshore waters, and smaller cells typical of the stations further offshore.

5 Conclusions

PI incubations were obtained from 15 stations extending from within King Sound into coastal waters, across the shelf towards offshore. This region of the shelf is subject to strong variations in water column stability associated with a tidal-mixing front distinguishing offshore stratified waters from well-mixed water on the shoreward side. Trends in the PI response and phytoplankton pigments demonstrate a partitioning of phytoplankton taxa associated with water column conditions either side of this tidal-mixing front. Shelf and offshore waters were characterised by smaller phytoplankton taxa eliciting a PI response consistent with stratified ocean conditions. The phytoplankton here have adapted their photo-physiology for the darker conditions encountered at the base of the euphotic layer, where a trade-off between light for photosynthesis and access to the deeper pool of nutrients yields the greatest success. In King Sound the phytoplankton community was comprised mostly of diatoms with the region identified as a pelagic productivity 'hotspot', despite reduced water clarity and low ambient nutrient concentrations compared with the adjacent shelf.

Here phytoplankton PI response displays low photosynthetic efficiency and an absence of photo-inhibition characteristic of light-adapted phytoplankton.

Remote sensing and numerical modelling suggest that spatial and temporal variations in tidal mixing drive changes in light variability and in photo-acclimation. Investigation of the photo-physiological response of the phytoplankton in King Sound, suggests that photo-acclimation to alternate weak and strong mixing exposes them to cyclical changes in light intensity delaying the onset of photo-inhibition. This allows higher maximum photosynthetic rates to be attained. Phytoplankton experience the largest variations in light over short timescales in King Sound where diatoms thrive since they have the capacity to rapidly acclimate to water column light conditions by adjusting pigment within the cell. This photo-acclimation strategy is responsible for the high rates of depth-integrated productivity measured in the estuary.

Acknowledgments

We would like to thank the CSIRO Wealth from Oceans Flagship for funding. We thank the captain and crew of RV *Southern Surveyor* and the Marine National Facility (MNF) staff for supporting the observational science. Nagur Cherukuru, Pru Bonham, and Peter Thompson (CSIRO) for pre and post cruise technical and analytical assistance. Lesley Clementson for phytoplankton accessory pigment sample analysis. Critical comments by Bozena Wojtasiewicz significantly improved the manuscript. All data and samples acquired on the voyage are made publicly available through the MNF repository found at https://www.marine.csiro.au/data/trawler/survey_details.cfm?survey=SS2010_V03 in accordance with MNF Policy. MODIS data was sourced from Australia's Integrated Marine Observing System (IMOS) which is enabled by the National Collaborative Research Infrastructure Strategy (NCRIS). Datasets used for this research are available in these in-text data citation references: Feng *et al.* (2017), IMOS (2020), McLaughlin *et al*. (2019) and Wijffels *et al*. (2018),

References

Auclair, J. C., Demers, S., Frechette, M., Legendre, L. 1982. High frequency endogenous periodicities synthesis in estuarine phytoplankton. Limnology 348-352.

Anon, 1972. Australia Pilot. In: North, North- West, and West Coasts of Australia from the West Entrance of Endeavour Strait to Cape Leeuwin, sixth ed., vol. 5 (Hydrographer of the Navy).

Behrenfeld, M. J., O'Malley, R. T., Boss, E. S., Westberry, T. K., Graff, J. R., Halsey, K. H., Milligan, A.J., Siegel, D.A., Brown, M.B. 2015. Revaluating ocean warming impacts on global phytoplankton. Nature Climate Change 6: 323–330.

Berges JA, Charlebois DO, Mauzerall DC, Falkowski PG (1996) Differential effects of nitrogen limitation on photosynthetic efficiency of photosystems I and II in microalgae. Plant Physiology 110: 689–696.

Berman-Frank I, Dubinsky Z (1999) Balanced growth in aquatic plants: myth or reality? Phytoplankton use the imbalance between carbon assimilation and biomass production to their strategic advantage. Bioscience 49: 29–37

Blain, S., Renaut, S., Xing, X., Claustre, H., Guinet, C. 2013. Instrumented elephant seals reveal the seasonality in chlorophyll and light-mixing regime in the iron-fertilized Southern Ocean: chlorophyll and light in Southern Ocean. Geophysical Research Letters 40: 6368–6372.

Blauw, A. N., Benincà, E., Laane, R. W., Greenwood, N., Huisman, J. 2012. Dancing with the tides: Fluctuations of coastal phytoplankton orchestrated by different oscillatory modes of the tidal cycle. PLoS One. 7: e49319.

Calbet, A., Agersted, M. D., Kaartvedt, S., Møhl, M., Møller, E. F., Enghoff-Poulson, S., Paulsen, M. L., Solberg, I., Tang, K. W., Tönnesson, K., Raitos, D. E., Nielsen, T. G. (2015) Heterogenous distribution of plankton within the mixed layer and its implications for bloom formation in tropical seas. Scientific Reports. 5 (11240). doi.org/10.1038/srep11240.

Cardol P., Bailleul B., Rappaport F., Derelle E. (2008) An original adaptation of photosynthesis in the marine green alga Ostreococcus. Proc Natl Acad Sci USA 105: 7881–7886

Cherukuru, N., Dekker, A.G., Hardman-Mountford, N.J., Clementson, L.A., Thompson, P.A. 2019. Bio-optical variability in multiple water masses across a tropical shelf: Implications for ocean colour remote sensing models. Estuarine, Coastal and Shelf Science 219: 223-230.

Clementson, L.A., Parslow, J.S., Turnbull, A.R., Bonahm, P. 2004. Properties of light absorption in a highly coloured estuarine system in south-east Australia which is prone to blooms of the toxic dinoflagellate Gymnodinium catenatum. Estuarine, Coastal and Shelf Science 60: 101-112.

Cloern, J.E., 1991. Tidal stirring and phytoplankton bloom dynamics in an estuary. Journal of Marine Research 49: 203-221.

Cresswell, G.R., Badcock, K.A. 2000. Tidal mixing near the Kimberley coast of NW Australia. Marine and Freshwater Research 51: 641-646.

de Boyer Montégut, C., Madec, G., Fischer, A.S., Lazar, A., Iudicone, D. 2004. Mixed layer depth over the global ocean: An examination of profile data and a profile-based climatology. Journal of Geophysical Research 109 (C12): 1-20.

Demers, S., Legendre, L. 1982. Water column stability and photosynthetic capacity of estuarine phytoplankton: long-term relationships. Marine Ecological Progress Series 7: 337-340

Demers, S., Legendre, L., Therriault, J. C. 1986. Phytoplankton reponses to vertical tidal mixing. In: Bowman, M. J., Barber, R. T., Mooers, C. N. K. (Eds), Lecture Notes on Coastal and Estuarine Studies. Springer-Verlag Publishing, New York, pp. 1-40.

Domingues, R. B., Anselmo, T. P., Barbosa, A. B., Sommer, U., Galvão, H. M. 2010. Tidal variability of phytoplankton and environmental drivers in the freshwater reaches of the Guadiana estuary (SW Iberia). International Review of Hydrobiology 95: 352–369.

Dubinsky, Z., Stambler, N. 2009. Photoacclimation processes in phytoplankton: mechanisms, consequences, and applications. Aquatic Microbial Ecology 56: 163–176.

Falkowski, P.G. 1980. Light and shade adaptation in marine phytoplankton. In: Primary Productivity in the Sea, pp. 99-119. P.G. Falkowski (ed.). Plenum Press, New York.

Falkowski, P.G. 1984. Physiological responses of phytoplankton to natural light regimes. Journal of Plankton Research 6: 295-307.

Falkowski, P.G., Laroche, J. 1991. Acclimation to spectral irradiance in algae. Journal of Phycology 27: 8-14.

Feng, M., Slawinski, D., Shimizu, K., Zhang, N. 2017. Climate change: knowledge integration and future projection. Final Report of Project 2.2.7 prepared for the Kimberley Marine Research Program, Western Australian Marine Science Institution, Perth, Western Australia, 50 pp.

Fischer, H. B. 1973. Longitudinal Dispersion and Turbulent Mixing in Open-Channel Flow. Annual Review of Fluid Mechanics, vol. 5, no. 1, 59–78.

Fréchette, M., Legendre, L. 1982. Phytoplankton photosynthetic response to light in an internal tide dominated environment. Estuaries 5: 287-293.

Hanson, C. E., Pesant, S., Waite, A. M., Pattiaratchi, C. B. 2007. Assessing the magnitude and significance of deep chlorophyll maxima of the coastal eastern Indian Ocean. Deep-Sea Research II 54: 884-901.

Herzig, R., Falkowski, P.G. 1989. Nitrogen limitation in Isochrysis galbana (Haptophyceae). 1. Photosynthetic energy conversion and growth efficiencies. Journal of Phycology 25:462–471.

Holloway, P.E., Chatwin, P.G., Craig, P. 2001. Internal Tide Observations from the Australian North West Shelf in Summer 1995. Journal of Physical Oceanography 31(5): 1182-1199.

Hooker, S.B., Van Heukelem, L., Thomas, C.S., Claustre, H., Ras, J., Schlüter, L. Clementson, L., Linde, D., Eker-Develi, E., Berthon, J-F., Barlow, R., Sessions, H., Ismail, H., Perl, J. 2009. The CSIRO method, in The Third SeaWiFS HPLC Analysis. Round-Robin Experiment (SeaHARRE-3). NASA Tech. Memo. 2009-215849, NASA Goddard Space Flight Center, Greenbelt, Maryland, 97 pp.

Houliez, E., Lizon, F., Artigas, L.F., Lefebvre, S., Schmitt, F.G., 2013. Spatio-temporal variability of phytoplankton photosynthetic activity in a macrotidal ecosystem (the Strait of Dover, eastern English Channel). Estuarine, Coastal and Shelf Science 129: 37-48.

IMOS. 2020. MODIS ocean colour satellite record from 2002 – 2020, https://portal.aodn.org.au/search?uuid=97b9fe73-ee44-437f-b2ae-5b8613f81042, accessed 14-04-2020.

Jeffrey, S.W., Vesk, M., 1997. Introduction to marine phytoplankton and their pigment signatures. In: Jeffrey, S.W., Mantoura, R.F.C., Wright, S.W. (Eds.), Phytoplankton Pigments in Oceanography: Guidelines to Modern Methods. UNESCO Publishing, Paris, pp. 37-84.

Jouenne, F., Lefebvre, S., Véron, B., Lagadeuc, Y. 2005. Biological and physiochemical factors controlling short-term variability in phytoplankton primary production and photosynthetic parameters in a macrotidal ecosystem (eastern English Channel). Estuarine, Coastal and Shelf Science 65: 421–439.

Kirk, J.T.O., Tilney-Bassett, R.A.E. 1978. The Plastids. Their chemistry, structure, growth and inheritance. Elsevier/North-Holland Biomedical Press, Amsterdam. 2nd edition. 960 pp.

Larkum, A.W., Vesk, M. 2003. Algal plastids: Their fine structure and properties. In Larkum, A.W., Douglas, S.E. Raven, J.A. (eds), Photosynthesis in algae, Kluwer Academic Publ, Dordrecht, The Netherlands, pp. 11-28.

Lavaud, J., Strzepek, R.F., Kroth, P.G. 2007. Photoprotection capacity differs among diatoms: Possible consequences on the spatial distribution of diatoms related to fluctuations in the underwater light climate. Limnology and Oceanography 52(3): 1188–1194.

Lewis, M.R., Smith, J.C., 1983. A small volume, short incubation-time method for measurement of photosynthesis as a function of incident irradiance. Marine Ecology-Progress Series 13: 99–102.

Lewis, M.R., Cullen, J.J., Platt T. 1984. Relationships between vertical mixing and photoadaptation of phytoplankton: similarity criteria. Marine Ecology Progress Series 15: 141-149.

Lewitus, A. J., Koepfler, E. T., Morris, J. T. 1998. Seasonal variation in the regulation of phytoplankton by nitrogen and grazing in a salt-marsh estuary. Limnology and Oceanography 43: 636–646.

Lourey, M.J., Thompson, P.A., McLaughlin, M.J., Bonham, P., Feng, M., 2012. Primary production and phytoplankton community structure during a winter shelf-scale phytoplankton bloom off Western Australia. Marine Biology 160: 355‑369.

Lucas, L.V., Koseff, J.R., Monismith, S.G., Cloern, J.E., Thompson, J.K., 1999. Processes governing phytoplankton blooms in estuaries. II: The role of horizontal transport. Marine Ecology Progress Series 187: 17-30.

Mackey, D.J., Parslow, J., Higgins, H.W., Griffiths, F.B., O'Sullivan, J.E., 1995. Plankton productivity and biomass in the western equatorial Pacific: biological and physical controls. Deep-Sea Research 42: 499–533.

Mackey, D.J., Parslow, J.S., Griffiths, F.B., Higgins, H.W., Tilbrook, B., 1997. Phytoplankton productivity and the carbon cycle in the western Equatorial Pacific under El Nino and non-El Nino conditions. Deep-Sea Research II 44: 1951–1978.

Marra, J., Lance, V.P., Vaillancourt, R.D., Hargreaves, B.R. 2014. Resolving the ocean's euphotic zone. Deep Sea Research 83: 45-50.

McLaughlin MJ, Lourey MJ, Hanson CE, Cherukuru N, Thompson PA, Pattiaratchi C. 2019. Biophysical oceanography of tidally-extreme waters of the southern Kimberley coast, Western Australia. Continental Shelf Research 173: 1-12.

Morel, A. 1991. Light and marine photosynthesis: a spectral model with geochemical and climatological implications. Progress in. Oceanography 26: 263–306.

Parsons, T.R., Maita, Y., Lalli, C.M., 1989. A Manual of Chemical and Biological Methods for Seawater Analysis. Pergamon Press, Toronto.

Platt, T., Gallegos, C.L., Harrison, W.G., 1980. Photoinhibition of photosynthesis in natural assemblages of marine phytoplankton. Journal of Marine Research 38: 687–701.

Sathyendranath, S., Watts, L., Devred, E., Platt, T., Caverhill, C., Maass, H., 2004. Discrimination of diatoms from other phytoplankton using ocean-colour data. Marine Ecology Progress Series 272: 59-68.

Savidge, G. 1979. Photosynthetic characteristics of marine phytoplankton from contrasting physical environments. Marine BioIogy 53: 1-12.

Simpson, J.H., Hunter, J.R. 1974. Fronts in the Irish Sea. Nature 250: 404-406.

Smetacek, V.S. 1985. Role of sinking in diatom life-history cycles: ecological, evolutionary and geological significance. Marine Biology 84: 239-251.

Smith R.C., Mobley C.D. 2008. Underwater light. In: Björn L.O. (ed) Photobiology: the science of life and light, 2nd edition. Springer, New York, p 131–138.

Trigueros, J.M., Orive, E., 2000. Tidally driven distribution of phytoplankton blooms in a shallow, macrotidal estuary. Journal of Plankton Research 22: 969–986.

Vidussi, F., Claustre, H., Manca, B.B., Luchetta, L., Marty, J. 2001. Phytoplankton pigment distribution in relation to upper thermocline circulation in the eastern Mediterranean Sea during winter. Journal of Geophysical Research 106: 19,939-19,956.

Vincent, W.F. 1980. Mechanisms of rapid photosynthetic adaptation in natural phytoplankton communities. II. Changes in photochemical capacity as measured by DCMU-induced chlorophyll fluorescence. Journal of Phycology 16: 568-577.

West, N.J., Scanlan, D.J. 1999. Niche-partitioning of Prochlorococcus populations in a stratified water column in the eastern North Atlantic Ocean? Applied and Environmental Microbiology 65: 2585-2591

Wetz, M.S., K.C. Hayes, A. J. Lewitus, J. L. Wolny, White, D.L. 2006. Variability in phytoplankton pigment biomass and taxonomic composition over tidal cycles in a salt marsh estuary. Marine Ecology Progress Series 320: 109–120.

Wijffels, S.E., Beggs, H., Griffin, C., Middleton, J.F., Cahill, M., King, E., Jones, E., Feng, M., Benthuysen, J.A., Steinberg, C.R., Sutton, P. 2018. A fine spatial-scale sea surface temperature atlas of the Australian regional seas (SSTAARS): Seasonal variability and trends around Australasia and New Zealand revisited. Journal of Marine Systems 187: 156-196.

Wolanski, E., Spagnol, S. 2003. Dynamics of the turbidity maximum in King Sound, tropical Western Australia. Estuarine Coastal and Shelf Science 56: 877-890.

Figures and Tables

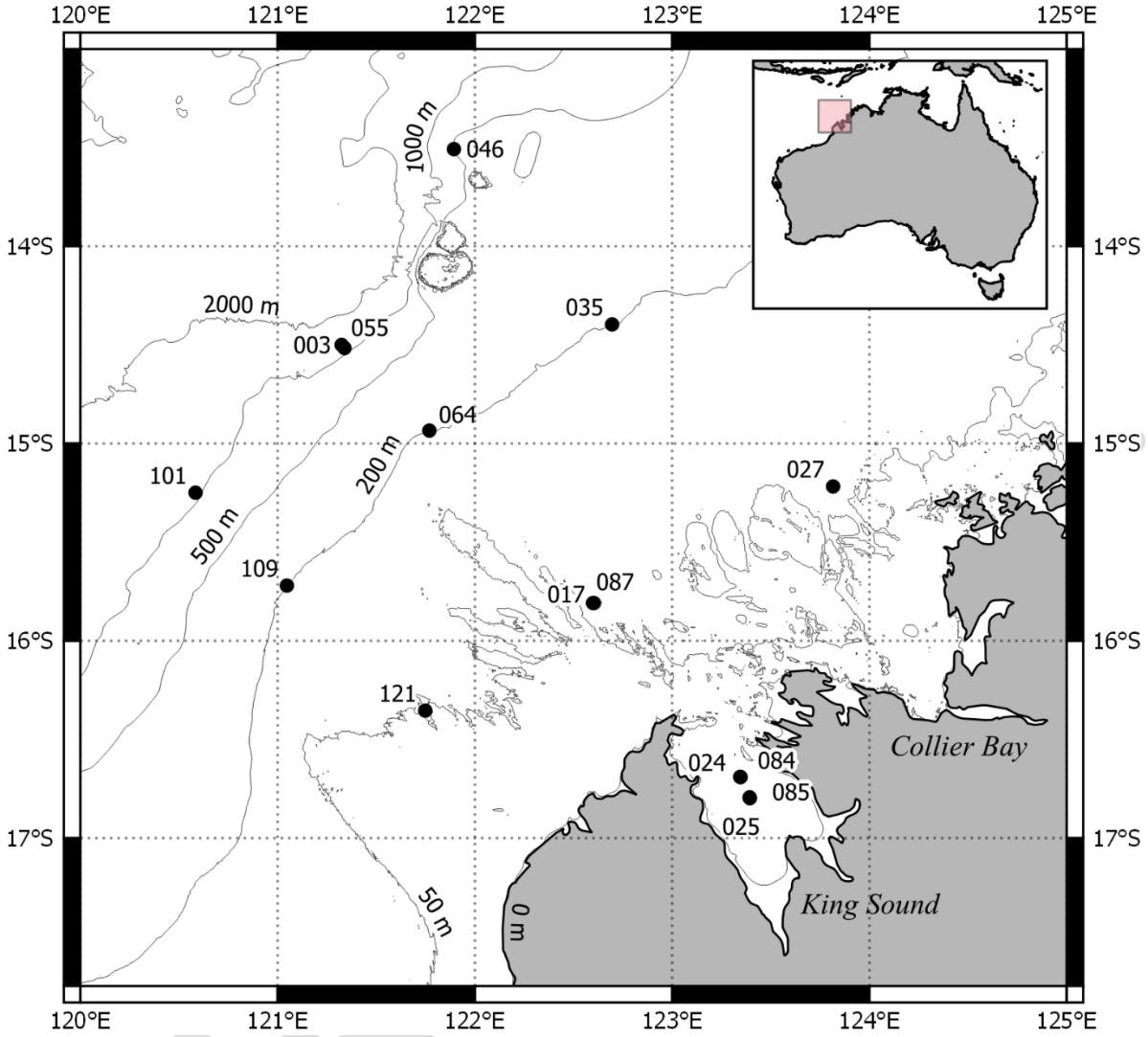

Fig 1. Location where phytoplankton productivity measurements, and supporting measurements of density, PAR, and chlorophyll fluorescence were made, within King Sound and on the adjacent shelf (solid circles).

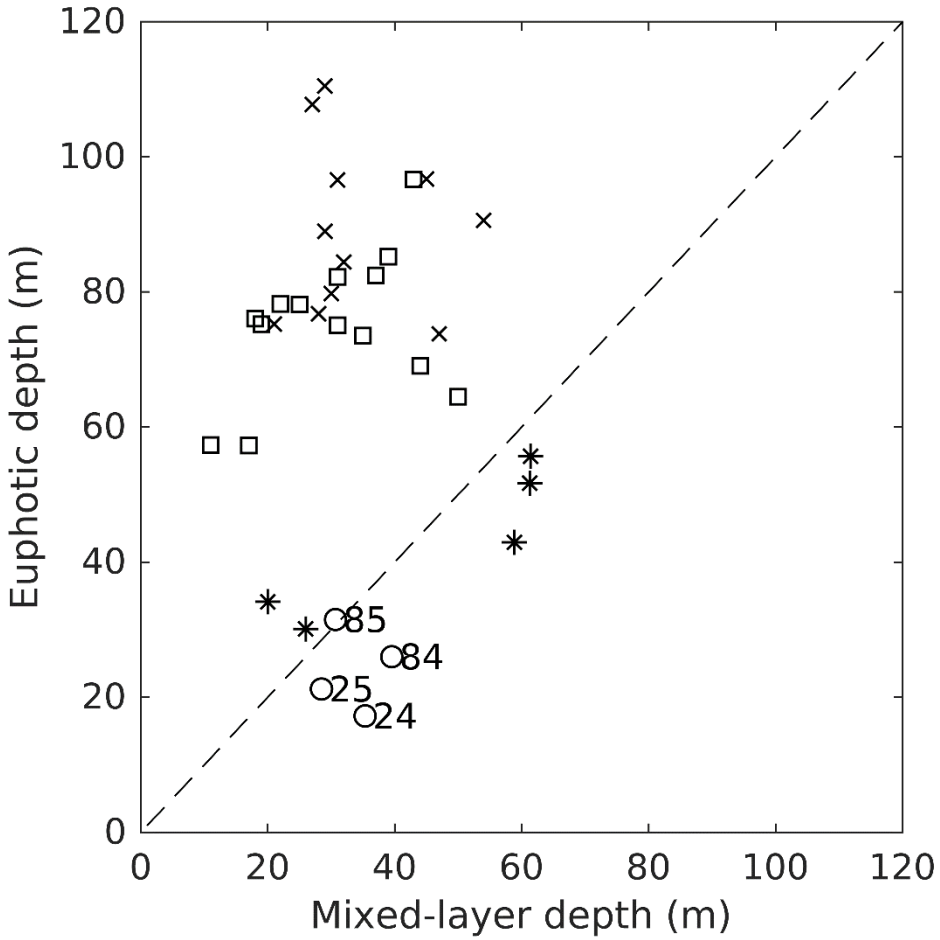

665

666 **Fig 2.** Variation of euphotic depth with mixed-layer depth at KS stations 24, 25, 84, and 85 (circles), and at
667 the 50 m (asterisks), 200 m (squares), and 1000 m (crosses) depth contours. The dashed line represents a
668 1:1 relationship between the two variables for reference.

669

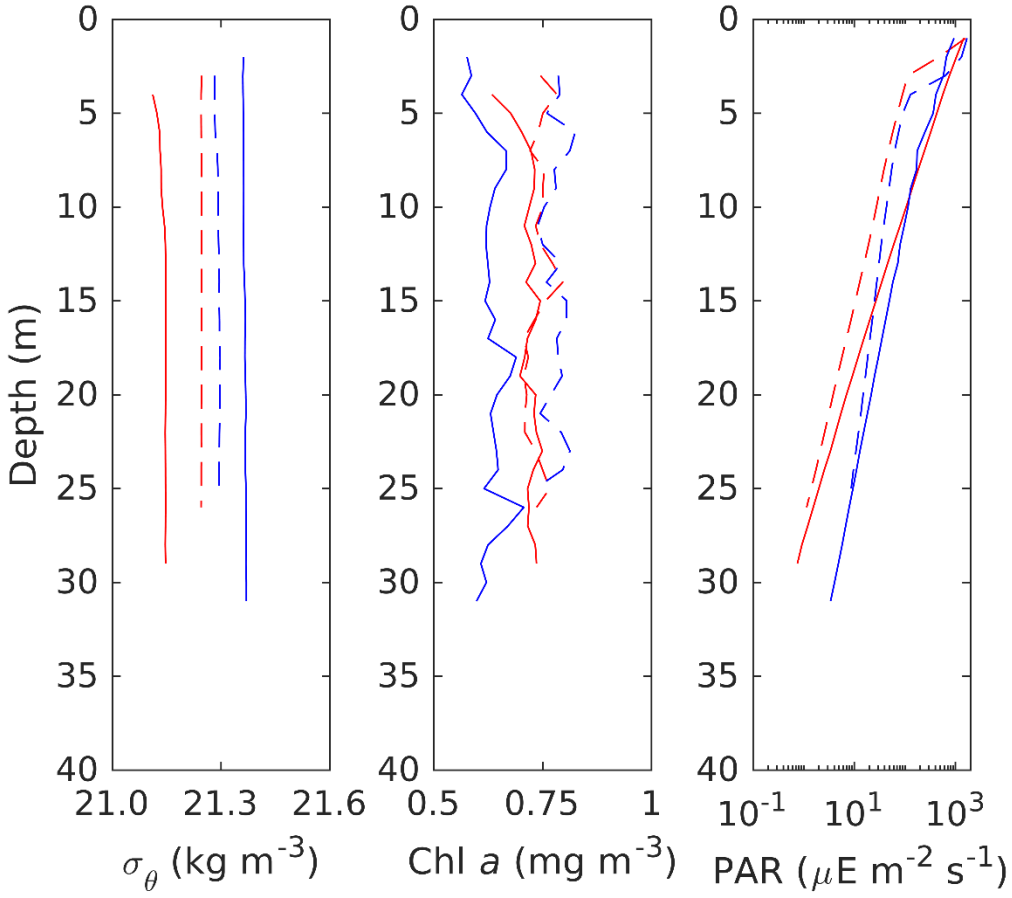

Fig. 3. Vertical variation in potential density (σ_θ), chlorophyll *a* concentration (Chl *a*), and natural logarithm of photosynthetic radiation (PAR) recorded at 1 meter vertical resolution during spring (solid lines) and neap (dashed lines) tide conditions for KS station 24 (red solid line), 25 (blue solid line), 84 (red dashed line) and 85 (blue dashed line).

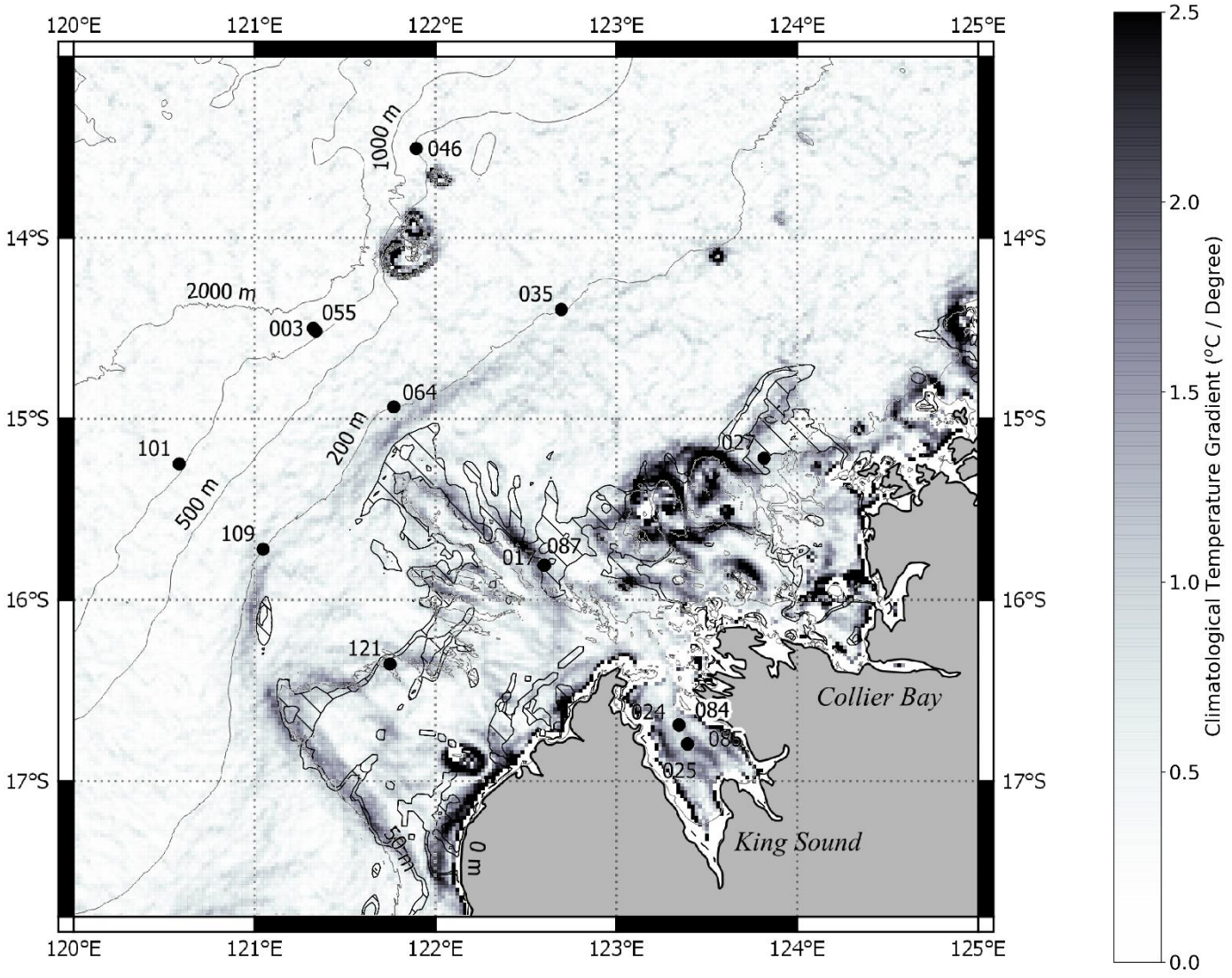

678

679 **Fig. 4.** Gradient in climatological temperature (shading) overlain with expected frontal region, $65 < h/{U_0}^3 <$
680 100, (hatched contours) calculated from the ROMS hydrodynamic model.

681

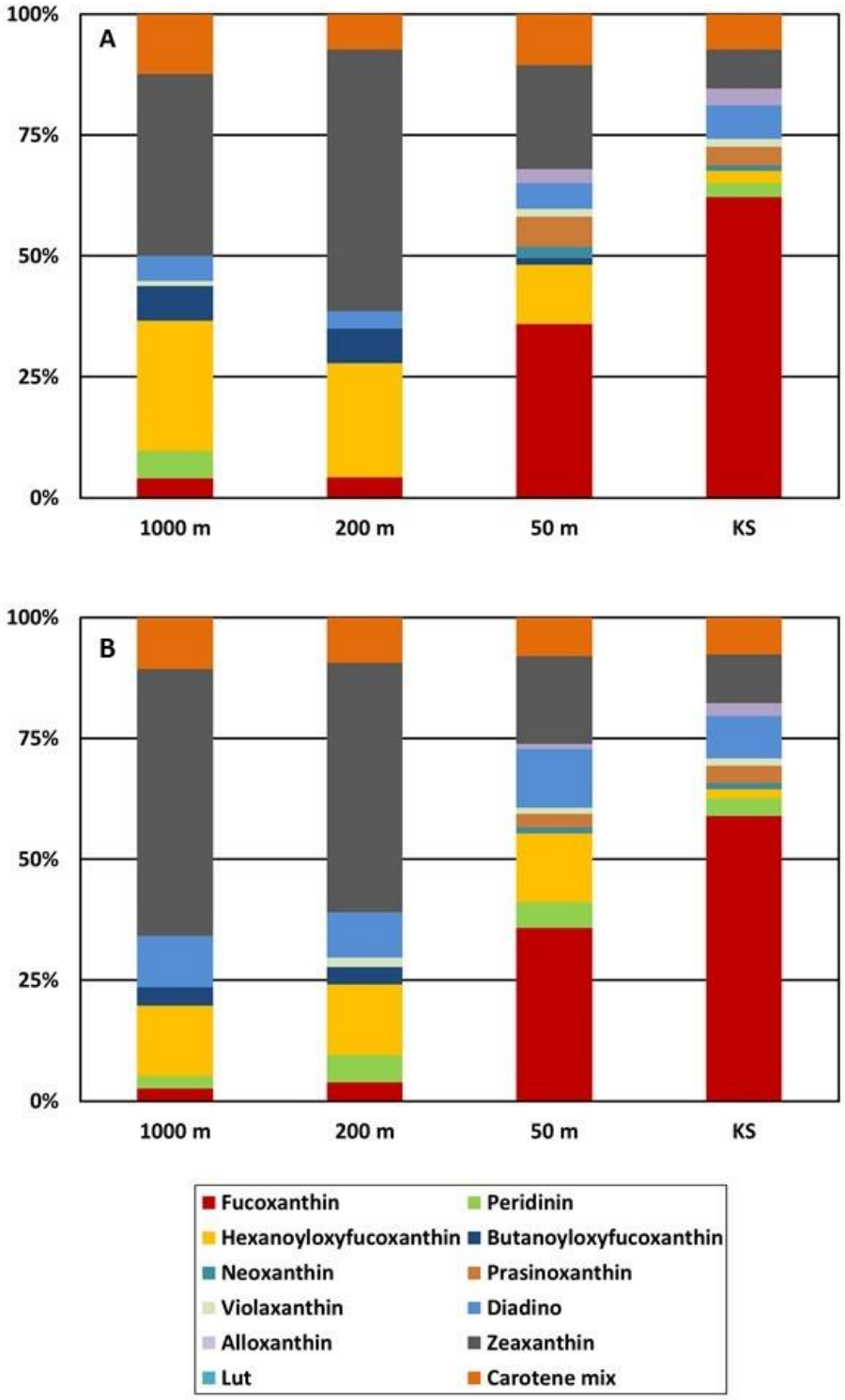

682

683 **Fig 5.** Variation of phytoplankton pigment concentrations in King Sound (KS), and at the 50, 200 and 1000
684 m depth contours on the adjacent continental shelf during (a) spring, and (b) neap tidal conditions (adapted
685 from McLaughlin *et al.*, 2019).

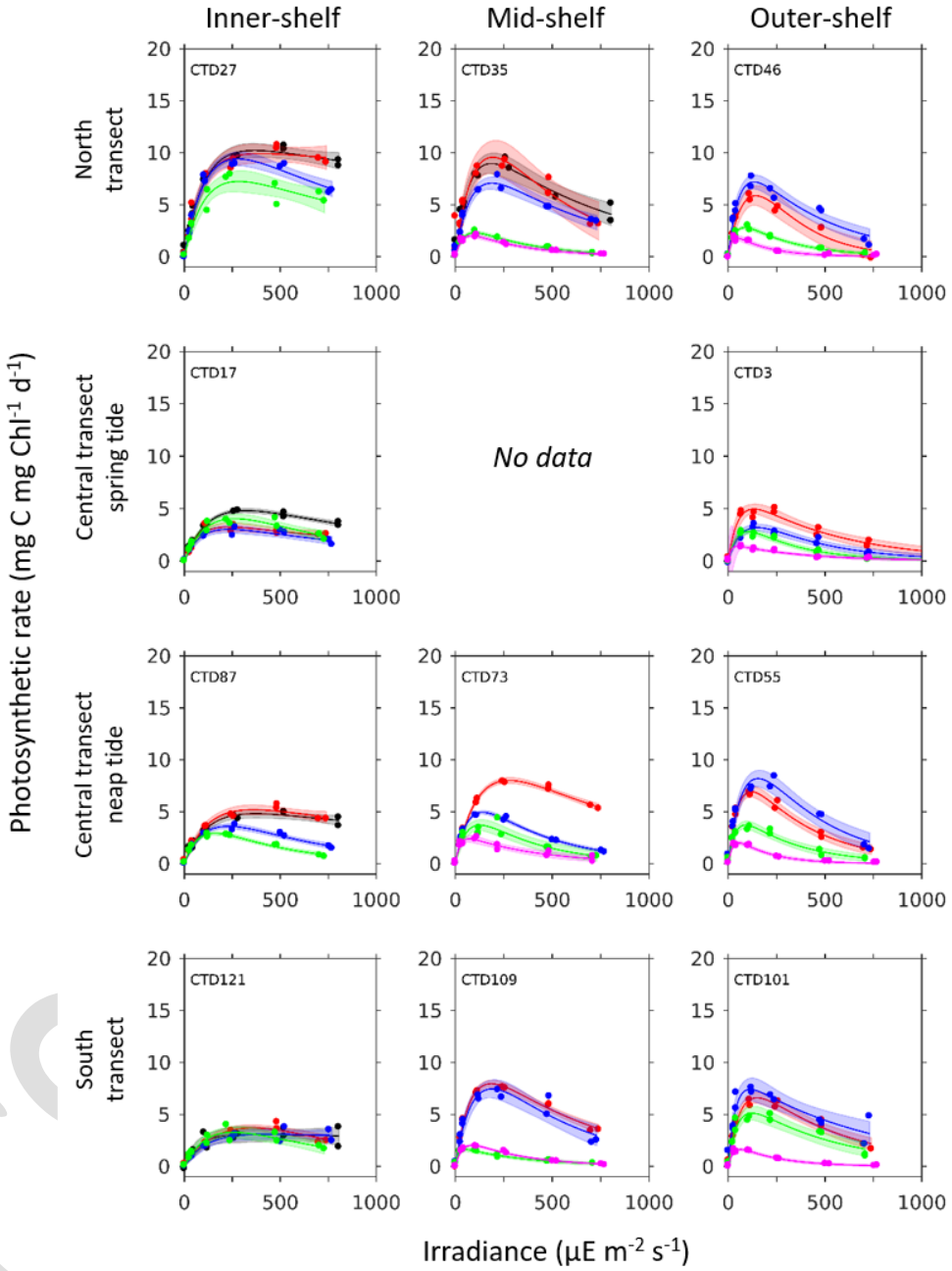

Fig. 6. Variation of photosynthetic rate with irradiance for inner-, mid-, and outer-shelf locations along the northern, central and southern transects shown in Fig 1. The code in the upper right corner of each panel indicates the CTD station number and corresponds with station numbers shown in figure 1, and used in table 1. Note that the central transect was sampled twice, once during spring tide conditions, and again during neap tide conditions. No data is available for the mid-shelf location sampled on the central transect during spring tide. Lines are a non-linear fitting of equation 1 to the data points (filled circles), and shading shows the 95% confidence interval of the fitting. Colours represent different vertical water-column positions: black 0 m, red 10 m, blue 25 m, green 50 m and magenta 75 m. Fitting parameters are reported in Table 1.

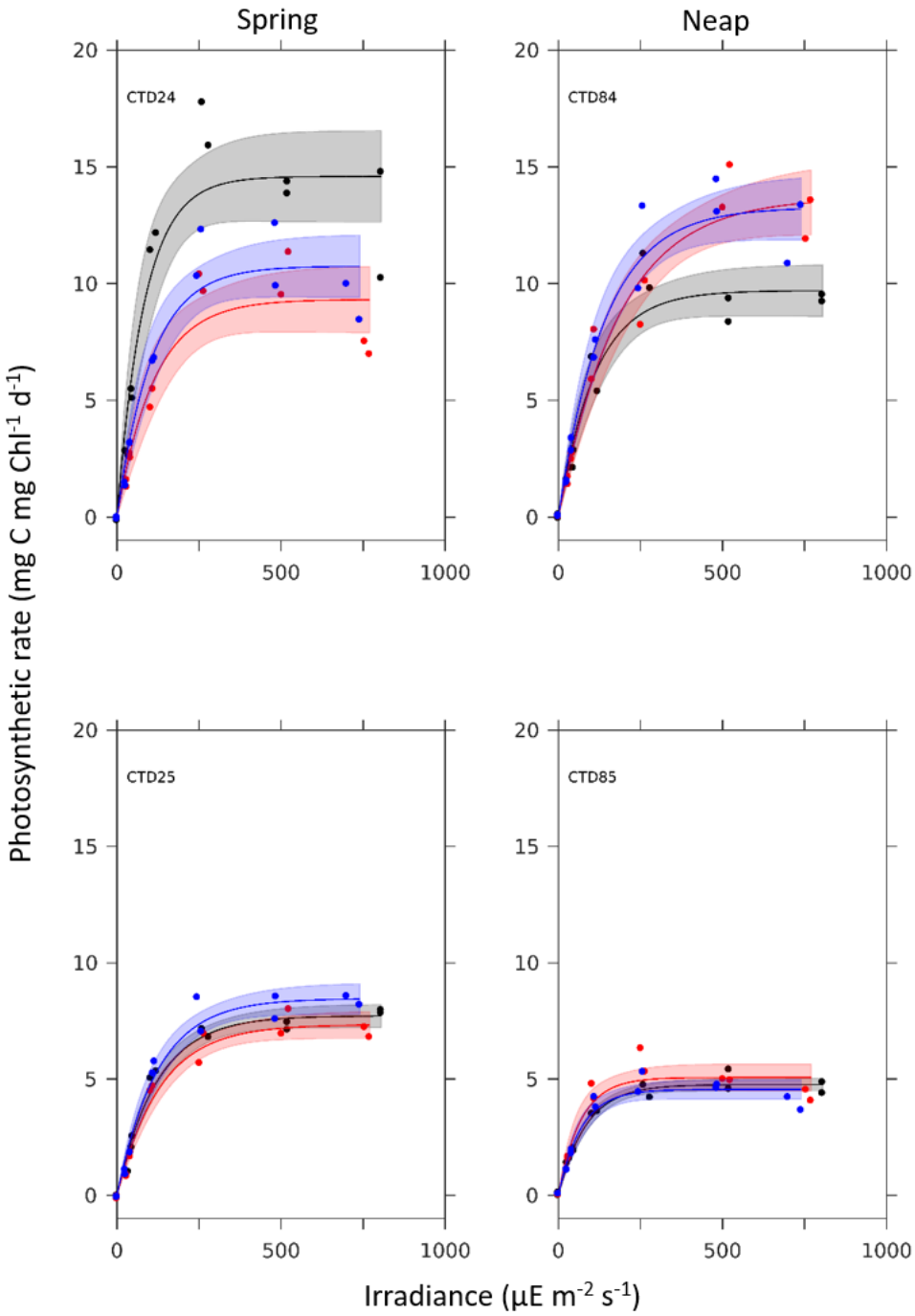

698

699 **Fig. 7.** Variation in photosynthetic rate with irradiance measured during spring (left-hand panels) and neap
700 (right-hand panels) tide conditions at two different locations (CTD 24/84, and CTD 25/85) within King Sound
701 (See Fig 1 for locations). Lines are a non-linear fitting of equation 3 to the data points (filled circles), and
702 shading shows the 95% confidence interval of the fitting. Colour represents different water-column depths:
703 black 0 m, red 10 m, and blue 25 m. Fitting parameters are reported in Table 1.

704

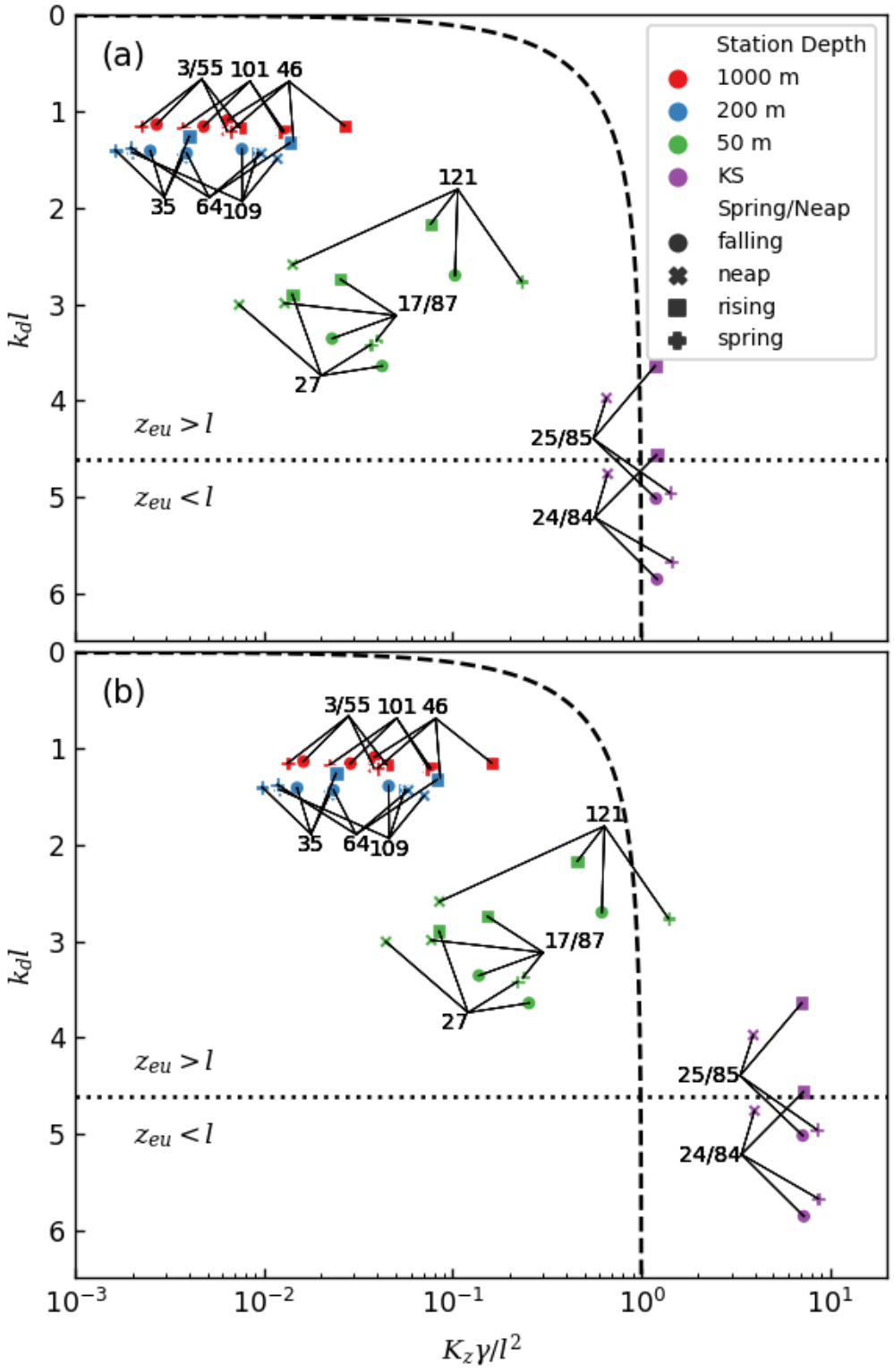

Fig. 8. Variation in photoadaptation regime at the sampling locations for stages of the spring-neap cycle in the non-dimensional parameter space of irradiance aspect ratio $k_d l$ and mixing timescale ratio $K_z \gamma / l^2$ for (a) photoadaptation time scale $\gamma = 4$ hours and (b) $\gamma = 24$ hours. The dashed line ($K_z \gamma / l^2 = 1 - \exp(-k_d l)$) divides the parameter space into a region where photoadaptation dominates and a region where vertical mixing dominates (Lewis *et al.*, 1984).

Table 1. K_d, Mean and Median PAR values as indicators of the light climate within the mixed layer depth for both Spring and Neap tidal influenced production stations located within King Sound.

Station	MLD (m)	Mixing Time Scale (h)	Kd ($m^{-1)}$	Mean PAR (mol photons $m^{-2}day^{-1}$)	Median PAR (mol photons $m^{-2}day^{-1}$)
24	36	3.6	0.27	48	4
25	29	3.5	0.22	74	20
84	40	6.6	0.18	66	13
85	31	6.6	0.15	101	48

714

Table 2. Fitted photosynthetic parameter value for each vertical water-column position sampled with shelf position.

CTD	Shelf position *(MS_f tidal phase)*	Seabed Depth (m)		MLD (m)	Parameter name	Fitted parameter value at each vertical water-column position sampled				
						0 m	*10 m*	*25 m*	*50 m*	*75 m*
24	King Sound *(spring)*	36		36	P_{max}	14.59	9.32	10.75	*Not applicable*	*Not applicable*
					α	0.18	0.08	0.10		
					β	-	-	-		
25	King Sound *(spring)*	29		29	P_{max}	7.72	7.34	8.46		
					α	0.06	0.06	0.07		
					β	-	-	-		
84	King Sound *(neap)*	40		40	P_{max}	9.70	13.69	13.26		
					α	0.09	0.07	0.09		
					β	-	-	-		
85	King Sound *(neap)*	31		31	P_{max}	4.77	5.07	4.55		
					α	0.06	0.08	0.07		
					β	-	-	-		
27	Inner shelf north transect	59		15	P_{max}	10.22	9.92	9.41	7.24	
					α	0.11	0.11	0.11	0.09	
					β	-	-	0.01	0.01	
17	Inner shelf central transect *(spring)*	62		62	P_{max}	4.81	3.24	3.02	4.04	
					α	0.05	0.05	0.04	0.05	
					β	0.01	-	-	0.01	
87	Inner shelf central transect *(neap)*	65		18	P_{max}	4.81	5.20	3.61	2.92	
					α	0.05	0.05	0.05	0.06	
					β	-	-	0.01	0.01	
121	Inner shelf south transect	62		61	P_{max}	3.07	3.23	3.09	3.27	
					α	0.04	0.04	0.03	0.04	
					β	-	-	-	0.01	
35	Mid shelf north transect	198		33	P_{max}	8.97	9.56	7.08	2.30	2.01
					α	0.16	0.15	0.12	0.07	0.08
					β	0.02	0.05	0.02	0.01	0.01
73	Mid shelf central transect *(neap)*	201		17	P_{max}	8.01	8.02	4.95	3.72	2.39
					α	0.09	0.09	0.11	0.09	0.12
					β	0.01	0.02	0.02	0.02	0.01
109	Mid shelf south transect	201		11	P_{max}	-	7.95	7.45	1.64	2.03
					α	-	0.14	0.12	0.13	0.08
					β	-	0.02	0.03	0.01	0.01
46	Outer shelf north transect	1007		45	P_{max}	-	5.87	7.19	2.80	1.80
					α	-	0.12	0.17	0.10	0.13
					β	-	0.10	0.03	0.02	0.01
3	Outer shelf central transect *(spring)*	1337		36	P_{max}	-	4.96	3.19	2.79	1.41
					α	-	0.12	0.06	0.08	0.11
					β	-	0.02	0.02	0.02	0.01
55	Outer shelf central transect *(neap)*	1049		52	P_{max}	-	6.93	8.19	3.72	2.00
					α	-	0.18	0.16	0.13	0.12
					β	-	0.03	0.04	0.02	0.02
101	Outer shelf south transect	1043		63	P_{max}	-	6.60	7.41	5.12	1.62
					α	-	0.14	0.24	0.14	0.08
					β	-	0.02	0.01	0.02	0.01

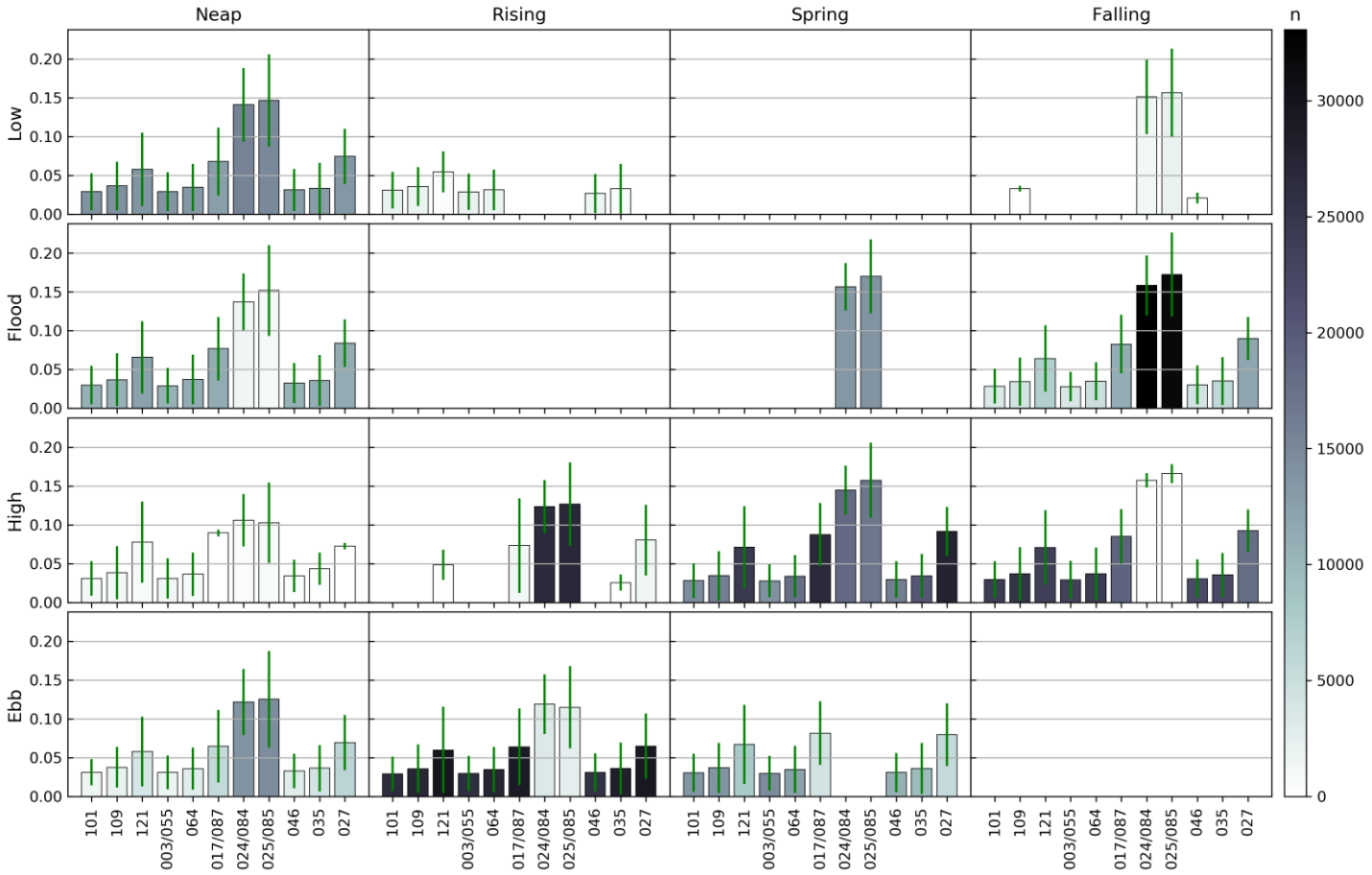

Fig. S1. Conditionally averaged MODIS k_d at 490 nm based on tidal phase of the semi-diurnal (high water, ebb tide, low water and flood tide) and spring-neap (spring, falling, neap and rising) cycles at the time of pixel acquisition. Cloud free pixels within 4 km of each station were utilised. Error bars show the 95% confidence interval of the mean and shading indicates the number of samples (n) within each class.